International Journal of Civil and Structural Engineering– IJCSE
Volume 2 : Issue 2 *[ISSN : 2372-3971]*
Publication Date: 19 October, 2015

Experimental Study on the Shear Strength of Steel Beams with Trapezoidal Corrugated Webs

[Samer Barakat, Ahmad Al Mansouri and Salah Altoubat]

***Abstract*—Steel beams with corrugated webs (CWSBs) have been shown theoretically and experimentally to have higher shear strength than beams with straight webs. A new formula is proposed to determine the shear strength of any trapezoidal CWSB based on its dimensions and material properties. The formula is numerically derived from the results of eight different experimental studies on the shear strength of trapezoidal CWSBs using multiple regression analysis (MRA). A set of eight trapezoidal CWSBs with three different web depths, two different web thicknesses, and two different angles of corrugation is fabricated. The beams were instrumented and tested to failure under center point load in simply supported configuration. The results showed that the failure mode was primarily due to web bucking way before material yielding which indicates that geometry of the corrugation plays a major role in the beam behavior. The new proposed formula is found to be in good agreement with the test results; the average ratio between the predicted and experimental shear capacities is found to be 1.06.**

***Keywords*—shear strength; regression; steel beams; trapezoidal corrugated web; experimental.**

I. Introduction

Obtaining Steel beams with corrugated webs are are typically composed of corrugated steel plates (forming the web) that are welded to a pair of flanges. The corrugations can take many shapes: rectangular, triangular, semi-circular, sinusoidal, and trapezoidal, the latter of which is the focus of this paper. Many theoretical and experimental studies have shown that steel beams with corrugated webs have higher shear strength than beams with straight webs, alleviating the need for transverse stiffeners. A number of studies have been carried out to quantify this effect, attempting to express the increase in shear strength of the section in terms of the geometry of the corrugations and the material properties (see for example [1]-[5]. This study aims at testing a formula derived in [6] from past experimental results to calculate the shear capacity of a trapezoidal CWSB with any given set of geometric and material properties using multiple regression analysis. To that end, a set of trapezoidal CWSBs is fabricated and tested to failure under shear. The test results are used to further check the accuracy of the formula.

Samer Barakat, Ahmad Al Mansouri, Salah Altoubat

Dept. of Civil and Environmental Engineering/University of Sharjah
UAE

II. Modes of shear buckling of CWSB

Fig. 1 shows an example of a trapezoidal corrugated steel beam and identifies all the relevant geometric properties for such a configuration: the length of the horizontal corrugation (a), the length of the horizontal projection of the diagonal corrugation (b), the length of the diagonal corrugation (c), the depth of the corrugation (d), the angle of corrugation (θ), and the thickness of the web (t_w).Two modes of shear buckling are defined: local and global buckling. Local buckling refers to deformations occurring in individual folds of the web [3]. These deformations can occur simultaneously in multiple folds and can propagate into adjacent unaffected folds. Global buckling, on the other hand, occurs over several folds, the buckled shape extending diagonally over the depth of the web. It is possible that an interaction between local and global buckling modes exist. The local $\tau_{L,el}$, global $\tau_{G,el}$and interactive$\tau_{I,n,el}$ elastic shear buckling stresses, can then be expressed as:

$$\tau_{L,el} = k_L \frac{\pi^2 E}{12(1-\nu^2)(w/t_w)^2} \tag{1}$$

$$\tau_{G,el} = k_G \frac{\left(D_y\right)^{1/4} \cdot (D_x)^{3/4}}{t_w \cdot h_w^2} \tag{2}$$

$$\tau_{G,el} = k_G F(\theta,\beta) \frac{E t_w^{1/2} b^{3/2}}{12 h_w^2} = C_G \frac{E t_w^{1/2} b^{3/2}}{12 h_w^2} \tag{3}$$

$$F(\theta,\beta) = \sqrt{\frac{1+\beta \sin^3\theta}{\beta+\cos\theta}} \cdot \left\{\frac{3\beta+1}{\beta^2(\beta+1)}\right\}^{3/4} \tag{4}$$

$$\tau_{I,n,el} = \frac{\tau_{L,el} \cdot \tau_{G,el}}{\left(\left(\tau_{L,el}\right)^n + \left(\tau_{G,el}\right)^n\right)^{1/n}} \tag{5}$$

$$\lambda_L = \sqrt{\frac{\tau_y}{\tau_{L,el}}} = \sqrt{\frac{12(1-\nu^2)\tau_y}{k_L \pi^2 E}} \frac{w}{t_w} \tag{6}$$

$$\lambda_G = \sqrt{\frac{\tau_y}{\tau_{G,el}}} = \sqrt{\frac{12\tau_y \cdot h_w^2}{k_G \cdot F(\theta,\beta) \cdot E \cdot t_w^{1/2} \cdot b^{3/2}}} \tag{7}$$

$$\lambda_{I,n} = \sqrt{\frac{\tau_y}{\tau_{I,n,el}}} = \lambda_L \lambda_G \left((1/\lambda_L)^{2n} + (1/\lambda_G)^{2n}\right)^{1/2n} \tag{8}$$

$$\tau_y = \frac{F_y}{\sqrt{3}} \tag{9}$$

$$D_y = \frac{b+d}{b+d \cdot \sec(\theta)} \cdot \frac{E \cdot t_w^3}{12} \tag{10}$$

$$D_x = \frac{E}{b+d}\left(\frac{b \cdot t_w \cdot (d \cdot \tan(\theta))^2}{4} + \frac{t_w \cdot (d \cdot \tan(\theta))^3}{12 \sin(\theta)}\right) \tag{11}$$

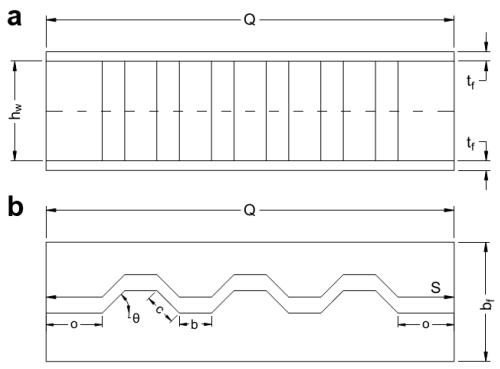

Fig. 1. (a) Profile of and (b) section through test beam.

where k_L is a coefficient that depends on the aspect ratio of the folds and the boundary conditions of the beam, E is Young's modulus, ν is Poisson's ratio, w is the fold width, and t_w is the thickness of the web. Of these values, only w, the fold width, changes from fold to fold. For longitudinal folds, $w = b$, and for inclined folds, $w = c$. The larger of b and c is taken to determine the smallest value of $\tau_{L,el}$. As fork_L, it is smallest when the ratio of w/h_w is small (where h_w is the height of the web) and when the beam is simply supported, taking a value of 5.34. Fixed support raises this value to 8.98, k_G is a coefficient that depends on the boundary conditions of the plate, k_G =31.6, assuming the flanges simply support the web, or 59, assuming the web is fixed to the flanges, θ is the angle of corrugation and d is the longitudinal projection of the inclined fold, as shown in Fig. 2,β is the ratio of b to c, θ is the corrugation angle usually ranges between 30° and 45°. In [6] the potential relationship between the experimental normalized shear buckling strength ρ_e and the slenderness ratio $\lambda_{I,1}$ (Eq. 8 with $n = 1$) was investigated (see Fig.2). The distribution of data points indicated a significant inversely proportional relationship between ρ_e and $\lambda_{I,1}$. Then a linear regression between ρ_e and $1/\lambda_{I,1}$ was performed and the results confirmed this relationship, producing an R^2 value of 0.934, as well as passing the F- and t-tests (see **Error! Reference source not found.**). Therefore, the best discovered regression model was as follows:

$$\rho_{n,S} = 0.747/\lambda_{I,1} \quad (12)$$

where

$$\lambda_{I,1} = \lambda_L \lambda_G \sqrt{((1/\lambda_L)^2 + (1/\lambda_G)^2)} \quad (13)$$

and λ_L and λ_G are as in Eqs.6 and 7, respectively.

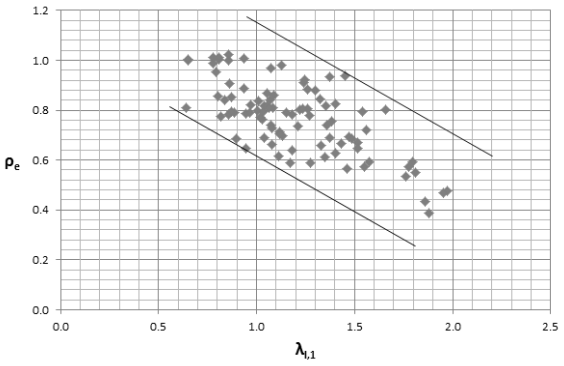

Fig. 2. Normalized shear buckling strength $\rho_e$vs. interactive slenderness ratio $\lambda_{I,1}$.

R^2	F-value		F-significance
0.930	956.704		0
Variable	Coefficient	t-value	t-significance
$1/\lambda_{I,1}$	0.747	30.931	0

Table 1. Nonlinear regression results

III. Experiment

To test the accuracy of the MRA model, CWSBs were fabricated and tested to failure under shear. The objective was to compare the experimental shear capacities to those predicted by the derived model [6]. Five beams were manufactured at a local steel workshop. Each beam consisted of two 150 mm wide and 12 mm-thick plates forming the flanges and a corrugated steel sheet forming the web. The dimensions of the beams are illustrated in Fig. 1 (a *= 70mm*, $b = c =$ *40mm*) and listed in Table 2.

Table 2. Dimensions of the test beams.

#	Identification	t_w (mm)	h_w (mm)	θ (°)	Q (mm)
1	A12-305-45	1.2	305	45	1193
2	A12-305-30	1.2	305	30	1294
3	A12-505-30	1.2	505	30	1294
4	A20-305-45	2	305	45	1193
5	A20-410-45	2	410	45	1193

Each web was welded to the flanges using a combination of continuous and intermittent welding. At the top of the beam, one side was welded continuously while the opposite was only welded at the interface between the longitudinal folds of the web and the flange. At the bottom of the beam, the same pattern was repeated in reverse. The result was that the top, bottom and both sides of the web each had one continuously welded and one intermittently welded edge. Fig. 3 shows the welding locations on a sample beam. In the absence of continuous welding throughout the beam, which was found to be too time-consuming and costly for this experiment, this technique ensures a strong bond between the web and flanges while distributing the strength of the bond as evenly as possible. The yield strength and modulus of elasticity of each of the two steel sheets from which the webs were cut were determined by performing tensile loading tests on three 10 mm by 40 mm strips of the same. The 1.2 mm and 2 mm-thick sheets were found to have mean yield strengths of 261 MPa and 661 MPa, respectively.

Figs. 4-6 show the experimental setup. The beams were simply supported and loaded at the center. An overhang of 70 mm past each support was provided to prevent the beams from slipping off the supports during testing.

Two strain gauges (SGs) were installed on either side of every beam at a quarter-span from each support, for a total of four strain gauges per beam. Linear variable differential transformers (LVDTs) were installed underneath each beam prior to testing at the locations indicated in Fig.4 to measure the deflection of the beam. The beams were loaded at a rate of 0.02 mm/s. Once the testing started, the force applied by the actuator was monitored continuously. Testing was stopped after the force had peaked and the web was observed to have buckled.

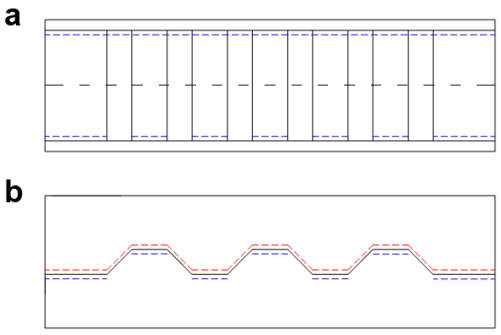

Fig. 1. Welding locations highlighted in blue and red on (a) profile of and (b) section through test beam.

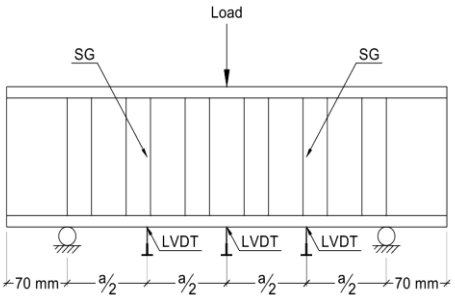

Fig. 2. Loading setup and locations of strain gauges (SG) and LVDTs.

Fig. 3. Profile of test beam with stiffeners.

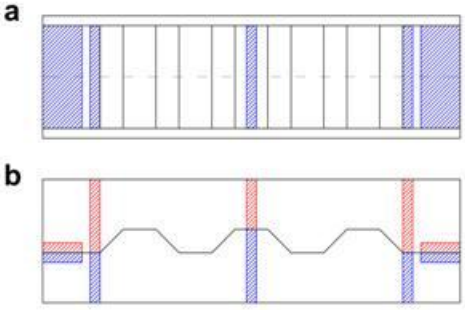

Fig. 4. Stiffener positions highlighted in blue and red on (a) profile of and (b) section through test beam.

Table 3 shows the shear capacities obtained from the five tested beams. Three degrees of web deformation were seen across these five beams. Beam A12-410-30, shown in Fig.7, exhibited the largest deformation, with numerous large creases propagating from the top left of the left panel to the bottom right of the same. All of the creases extended at least half way down the depth of the web, and several reached the bottom flange. Beams A12-505-30 and A12-505-45, depicted in Figs.8 and 9, both experienced moderate web deformation, with numerous large but shallow creases traveling in the same direction as in the previous beam. In both cases, only one or two creases appeared to reach the center of the depth of the web. The other creases remained near the top of the beam. Beams A12-305-45 and A12-410-45 did not deform as the previous three beams did, acquiring a single large, deep crease each rather than several smaller ones, as shown in Figs. 10 and 11. The distinction between these different types of deformation is reflected in the force-displacement plots of the corresponding tests shown in Fig. 12. The plot of beam A12-410-30 reveals many peaks and troughs in the plastic region, suggesting that some folds of the web continue to provide strength even after the web as a whole has buckled. This indicates the presence of interactive buckling, as the various folds of the web act as a whole (global buckling) as well as individually (local buckling).

Table 3: Experimental shear capacities of the tested beams.

#	Identification	Experimental shear capacity V_e (kN)
1	A12-305-45	53.85
2	A12-410-30	66.30
3	A12-505-30	72.01
4	A12-410-45	73.81
5	A12-505-45	81.36

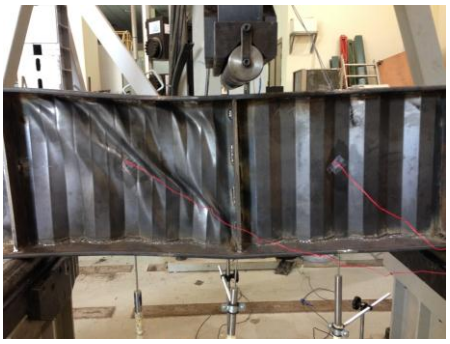

Fig. 5: Profile of beam A12-410-30 after loading-buckled panel.

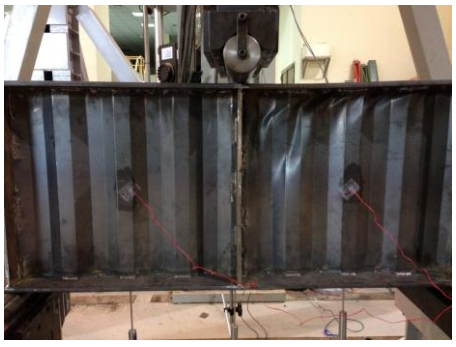

Fig. 6: Profile of beam A12-505-30 after loading-buckled panel.

Fig. 7: Profile of beam A12-505-45 after loading-buckled panel.

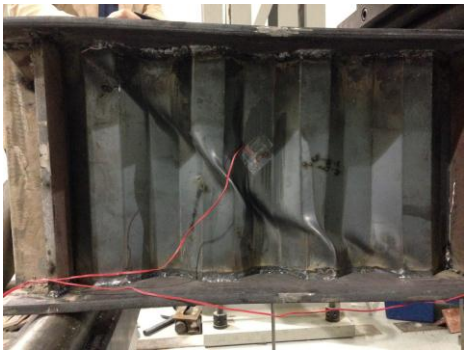

Fig. 10: Profile of buckled panel of beam A12-305-45.

Fig.11: Profile of beam A12-410-45 a) after loading. b) buckled panel.

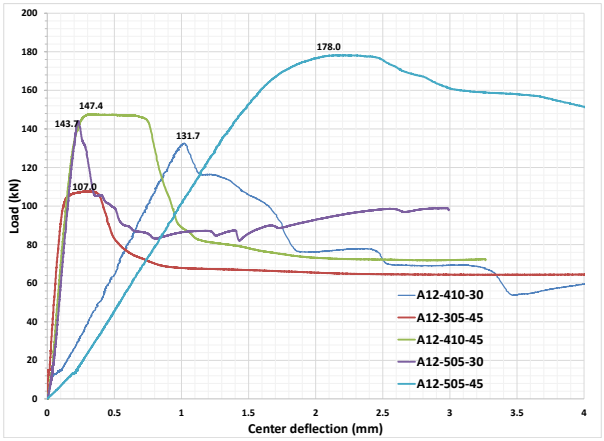

Fig. 12: Force-displacement graph of the tested beams.

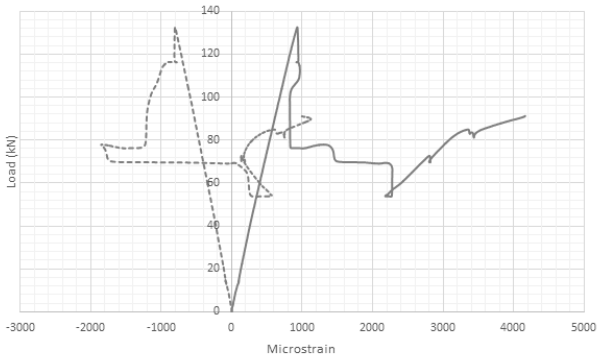

Fig. 8. Load-strain graph of beam A12-410-30.

The force-displacement plot of beam A12-410-30 is in sharp contrast to that of beams A12-305-45 and A12-410-45, which show plateaus in the plastic region. Here, the beams appear to work as a whole rather than a series of connected folds, exhibiting the same behavior that would be a seen in non-corrugated web beams. The plots of beams A12-505-30 and A12-505-45, depict the same kind of behavior as that of beam A12-410-30, but to a lesser degree; the peaks and troughs are less pronounced and there are fewer of them. This is explained by the deeper webs of the former two; the creases did not travel far down the web before the beam yielded, suggesting that the lower aspect ratio (a/h_w) of these beams is not as efficient as that of beam A12-410-30.

A study of the load-strain graphs (A12-410-30 in Fig. 8) of the tested beams reveals that they buckled before the yield strain (ε_y) of the material, which was 2115 μstrains for the 1.2mm-thick sheet, was reached. The graph shows the strain measured on either side of the buckled panel of the corresponding beam. Table 4 lists the experimental strain $(\mu\varepsilon_e)$ that corresponds to the peak load for each beam and compares it to the yield strain $(\mu\varepsilon_y)$.Two points are clear from design of the beams doesn't take full advantage of the strength of the material. 2) Beams with 45° corrugations reach a higher strain at the point of buckling than those with 30° corrugations (experimental-to-yield strain ratios of 0.555 and 0.507 for the former compared to 0.440 and 0.386 for the latter). This indicates that 45° corrugations are more efficient than 30° corrugations.

Table 4 compares the experimental shear capacities (V_e) of the five successfully tested beams with the shear capacities predicted by the proposed model [6] (V_S) and Sause and Braxtan's [5] (V_B). Table 4 makes clear several points: The new formula (V_S) predicted the test results more accurately than the one proposed by Sause and Braxtan (V_B); the former has an average predicted-to- experimental shear capacity ratio (V_S/Ve) of 1.06, whereas the latter's (V_B/Ve) is 0.87. V_B is less precise than V_S; from the comparison shown in Fig.14, it can be seen that the results of V_B are more dispersed with regard to the equality line, whereas those of V_S are clustered tightly together. V_S is not conservative; it always overestimates the shear capacity, whereas V_B always underestimates it.

Table 4. Comparison of yield strain with experimental strain

: 1)The geometry of the beams is inefficient; the average strain measured at the point of buckling is less than half of the yield strain ($\mu\varepsilon_e/\mu\varepsilon_y = 0.472$). This suggests a

geometric rather than material failure, and means that the design of the beams doesn't take full advantage of the strength of the material. 2) Beams with 45° corrugations reach a higher strain at the point of buckling than those with 30° corrugations (experimental-to-yield strain ratios of 0.555 and 0.507 for the former compared to 0.440 and 0.386 for the latter). This indicates that 45° corrugations are more efficient than 30° corrugations.

Table 4 compares the experimental shear capacities (V_e) of the five successfully tested beams with the shear capacities predicted by the proposed model [6] (V_S) and Sause and Braxtan's [5] (V_B). Table 4 makes clear several points: The new formula (V_S) predicted the test results more accurately than the one proposed by Sause and Braxtan (V_B); the former has an average predicted-to- experimental shear capacity ratio (V_S/Ve) of 1.06, whereas the latter's (V_B/Ve) is 0.87. V_B is less precise than V_S; from the comparison shown in Fig.14, it can be seen that the results of V_B are more dispersed with regard to the equality line, whereas those of V_S are clustered tightly together. V_S is not conservative; it always overestimates the shear capacity, whereas V_B always underestimates it.

Table 4. Comparison of yield strain with experimental strain
Table 4. Comparison of test results with predicted results.

#	V_e (kN)	V_S (kN)	V_B (kN)	V_S/V_e	V_B/V_e	$V_{S,c}$ (kN)	VS,c/Ve
1	53.9	64.5	43.5	1.19	0.81	60.1	1.12
2	66.3	67.0	57.9	1.01	0.87	62.3	0.94
3	72.0	72.3	69.6	1.00	0.97	67.2	0.93
4	73.8	77.6	58.4	1.05	0.79	72.1	0.98
5	81.4	86.1	71.6	1.06	0.88	80.1	0.98
			Average V/V_e =	**1.06**	**0.87**		0.99

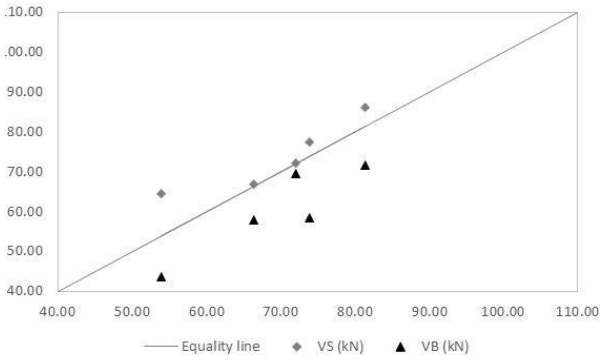

Fig.14. Comparison of test result with predicted results.

The first point suggests that the proposed model is more accurate than that of Sause and Braxtan [11], even though all five of the beams fall squarely within the boundaries set by them for their formula ($a/h_w > 1$, $\theta \geq 22°$, $0.87 \leq \beta \leq 1.13$). Furthermore, while the new formula is approximately 7.2% more accurate within that range, it is not limited to it, and is meant to return consistent results for any combination of dimensions. This is evident in14; the spread of the results of V_B is almost twice as large as that of V_S, indicating higher variance in the former. Finally, as the proposed model was developed through linear regression and with accuracy as the main concern, the practical issue of a safety margin was overlooked. The higher values predicted by the formula indicate that it is not conservative for at least a small range of configurations. Further investigation is required to determine the breadth of this range. Consequently, a final correction factor might be needed under some conditions to ensure the formula is safe for design. Table 5 (columns 7 and 8) shows the results of applying a preliminary correction factor of 0.93 to the proposed model. The average ratio of predicted to experimental shear capacity is reduced from 1.06 to 0.99, making the model conservative and more accurate by 5.4% on average. However, this correction factor is an initial estimate and is derived from the results of only 5 tests; it cannot be recommended before studying its results on a larger sample. Further experiments on a more diverse range of configurations are needed to prove this point. Moreover, the test results proved that the design of the beams is inefficient; all of the beams buckled far before the yield point of the material was reached. More investigation is needed to find out whether this is due to the nature of CWSBs in general, the specific geometries of the tested beams, manufacturing imperfections, or testing conditions. The test results also suggested that some angles of corrugation might be more efficient than others. It would be beneficial to conduct an optimization study of CWSBs to find the most efficient combination of angle of corrugation and longitudinal/inclined fold ratio.

IV. Summary and Conclusions

This work aimed to study the shear buckling strength of CWSBs. To that end, a total of 93 experimental data points were collected from different sources and randomly assigned to one of two sets. Mathematical models for the key response parameter (shear buckling strength of a CWSB) were established via MRA in terms of different input geometric, loading and materials parameters. A number of different models were tested before settling on one that produced satisfactory results. The final model had an R^2 value of 0.93 and passed the F- and t-tests. With this model, it is possible to predict the shear buckling strength of CWSBs from their geometric and material properties with good accuracy. A set of five CWSBs were fabricated and tested to failure under shear. The test results showed satisfactory agreement with the predicted results of the MRA model; the average ratio between the predicted and experimental shear capacities was found to be 1.064. Better manufacturing standards and a wider range of beam configurations are needed to evaluate the effectiveness of the new model using the experimental approach.

References

[1] R. Sause, H. H. Abbas, W. Wassef, R. Driver and M. Elgaaly, Corrugated web girder shape and strength criteria : work area 1, Pennsylvania innovative high performance steel bridge demonstration project, Bethlehem (PA): ATLSS Engineering Research Center, Lehigh Univ., 2003.

[2] R. G. Driver, H. H. Abbas and R. Sause, "Shear behavior of corrugated web bridge girders," Journal of Structural Engineering, vol. 132, no. 2, p. 195–203, 2006.

[3] J. Yi, H. Gil, K. Youm and H. Lee,"Interactive shear buckling behavior of trapezoidally corrugated steel webs," Engineering Structures, vol. 30, no. 6, p. 1659–1666, 2008.
[4] J. Moon, J. Yi, B. H. Choi and H.-E. Lee, "Shear strength and design of trapezoidally corrugated steel webs," Journal of Constructional Steel Research, vol. 65, no. 5, p. 1198–1205, 2009.
[5] R. Sause and T. N. Braxtan, "Shear strength of trapezoidal corrugated steel webs," Journal of Constructional Steel Research, vol. 67, no. 2, pp. 223-236, 2011.
[6] S. Barakat, A. Al Mansouri and S. Altoubat, ”Shear strength of steel beams with trapezoidal corrugated webs using regression analysis,” Steel and Composite Structures, vol. 18, no.3, 2015, DOI: http://dx.doi.org/10.12989/scs.2015.18.3.000
[7] J.-G. Niea, L. Zhu, M.-X. Tao and L. Tang, "Shear strength of trapezoidal corrugated steel webs," Journal of Constructional Steel Research, vol. 85, no. 1, p. 105–115, 2013.
[8] T. Guo and R. Sause, "Analysis of local elastic shear buckling of trapezoidal corrugated steel webs," Journal of Constructional Steel Research, vol. 102, no. November, pp. 59-71, 2014.